RSC Advances

This article can be cited before page numbers have been issued, to do this please use: P. Mierczynski, A. Mierczynska-Vasilev, W. Maniukiewicz, T. P. Maniecki and K. Vasilev, *RSC Adv.*, 2016, DOI: 10.1039/C6RA15618E.

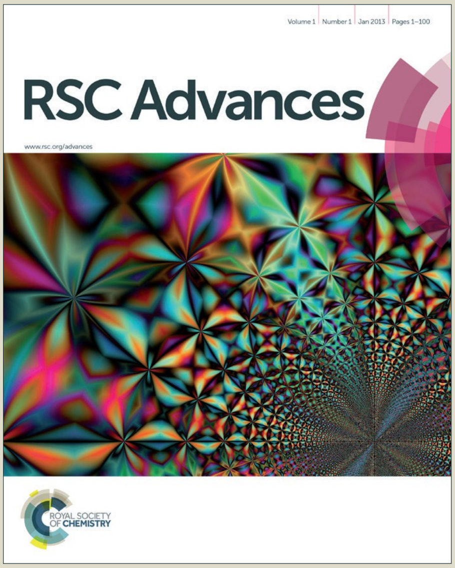

ROYAL SOCIETY
OF CHEMISTRY

www.rsc.org/advances

View Article Online
DOI: 10.1039/C6RA15618E

Journal Name

COMMUNICATION

MWCNTs as a catalyst in oxy-steam reforming of methanol

P. Mierczynski[a], A. Mierczynska[c], W. Maniukiewicz[a], T.P. Maniecki[a] and K. Vasilev[b]

Received 00th January 20xx,
Accepted 00th January 20xx

DOI: 10.1039/x0xx00000x

www.rsc.org/

The catalytic activity of multi-walled carbon nanotubes (MWCNTs) in oxy-steam reforming of methanol (ASRM) was invesigated for the fist time. We demonstrate that CNTs can present a potent catalitic material for hydrogen generation in oxy-steam reforming of methanol.

Tackling climate change, one of the greatest challenges today, requires a broad portfolio of renewable energy sources [1-3]. One possible energy carrier is hydrogen. It offers high gravimetric energy density and zero emission during combustion or conversion in fuel cells[4]. The use of hydrogen as a fuel for transportation and stationary applications has received much attention[5]. Hydrogen is being explored for use in internal combustion (IC) engines and fuel cell electric vehicles[6, 7]. Fuel cells technology is in the early stages of commercialization and offers a more efficient hydrogen use over hydrogen-fuelled IC engines. Hydrogen and fuel cells are often considered as a key technology for future sustainable energy supply. In comparison to traditional methods for electric energy generation from coal, fuel cells have lower carbon dioxide emission and about reduction of nitrogen oxides emission, which can have significant influence on the environment[8-10].

In light of the potential of hydrogen as a future energy source, novel catalyst concepts for methanol steam reforming are extensively investigated. Recently, carbon nanotubes (CNTs) and active carbon have attracted attention as novel catalyst support materials[11]. Solymosi et al.[12] studied group 8-10 metals immobilized on active carbon and carbon nanotubes in the decomposition and steam reforming of methanol. These catalysts suffered from low selectivity to carbon dioxide. Lio and Yang prepared Cu/ZnO on CNT catalysts and applied them to methanol steam reforming[13]. High activity and selectivity was reported for the temperature range of 200 to 400 °C.

The interest in using CNTs as catalysts or/and catalyst support stems from the material high thermal and mechanical stability and unique electron structure. In addition, the good conductivity of CNTs is thought to promote a spillover effect between active phase and support[14]. The interaction between the metal and support, specific electron structure and the presence of active nanoparticles both inside and on external wall of carbon nanotubes make then a very promising material as catalyst support[15]. Furthermore, nanoparticles dispersed on the support surface present active centres easily accessible to the reactants.

However, despite of these few studies concerned with metal catalysts supported on carbon nanotubes, the intrinsic catalytic properties of carbon nanotubes have never been explored in the oxy-steam reforming of methanol reaction (ASRM).

In the present work, multi-walled carbon nanotubes (MWCNTs) synthesized by chemical vapour deposition (CVD), both as synthesised and after purification, were investigated for their potential as catalysts in ASRM. To the best of the knowledge of the authors, this is the first time pristine MWCNTs containing iron species (α-Fe_2O_3, Fe_3C) or activated synthesized systems (containing Fe_3C, Fe_3O_4, Fe) were used alone as catalysts in ASRM reaction.

The aim of this work was to develop a new simple and efficient catalysts nanosystem consisting only of MWCNTs which can be utilized in hydrogen production from methanol. Methanol represents a potential carrier for the convenient storage of hydrogen, a novel catalytic concepts for hydrogen generation from methanol is of particular importance.

Multi-walled carbon nanotubes were synthesized by chemical vapour deposition (CVD) at 850 °C using ferrocene as a catalyst. The scanning electron microscopy (SEM) and transmission electron microscopy (TEM) images (see Fig. 1) showed that the nanomaterial is composed of carbon nanotubes aligned perpendicularly to the carpet basis which is contaminated with iron oxide (III) (hematite) particles and iron carbide (cementite) originating from the ferrocene catalyst. The SEM results showed that nanotube length (i.e. carpet height) is in the range of 440 - 460 µm. TEM observations on dispersed sample reveal that the nanotubes are multi-walled having outer and inner diameters of approximately 30-60 nm, and in the 8-10 nm, respectively. The TEM images also reviled the presence of iron-based particles of hematite (Fe_2O_3) and cementite (Fe_3C) (Fig. 1).

---

[a] Lodz University of Technology, Institute of General and Ecological Chemistry 90-924 Lodz, Poland, Zeromskiego 116, e-mail*- mierczyn25@wp.pl, pawel.mierczynski@p.lodz.pl tel: 0048-42-631-31-25, fax: 0048-42-631-31-28.

[b] School of Engineering, University of South Australia, Mawson Lakes, SA 5095, Adelaide, Australia. e-mail - Krasimir.Vasilev@unisa.edu.au

[c] The Australian Wine Research Institute, P.O. Box 197,Glen Osmond (Adelaide), SA 5064, Australia.

View Article Online
DOI: 10.1039/C6RA15618E

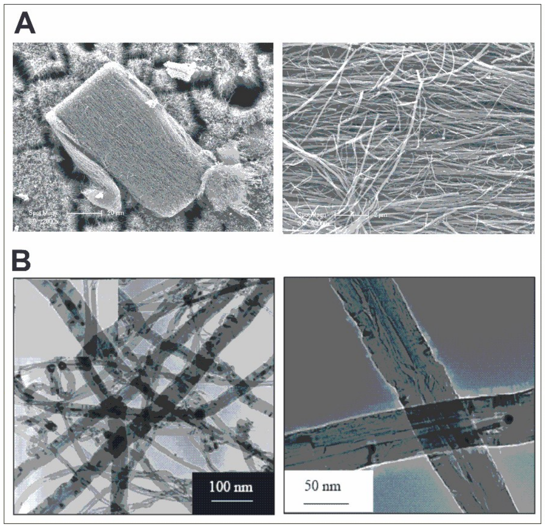

Fig.1 SEM (A) and TEM (B) images of multi-walled carbon nanotubes collected from the reactor.

The presence of nanoparticles inside the tubes suggests that the carbon nanotubes stabilize the Fe_2O_3 and/or Fe_3C. Furthermore, the presence of iron based particles suggests that iron (III) oxide is bounded by strong interaction inside the tubes and that the nanoparticles are encapsulated inside of the MWCNTs.

The type of iron species e.g. hematite, metallic iron, and magnetite that can be present in the MWCNTs may play a curial role in oxy-steam reforming of methanol. To elucidate the role of these iron based additives on the catalytic performance, the synthesised MWCNTs we subjected to different treatment: reduction at 500 °C in 5%H_2-95%Ar atmosphere, purification with concentrated HCl as reported by Edwards et al. [16] in order to remove iron based impurities, and purification and reduction.

In order to ensure that the systems under investigation are stable at the reaction temperature, thermal stability measurements were performed for purified and pristine MWCNTs. Both systems were reduced at 500 °C in a mixture 5%H_2-95%Ar MWCNTs (Fig. S1 and S2, ESI†). The TG results showed that purification of MWCNTs had a substantial influence on the nanomaterial stability. Carbon nanotubes, which were purified in concentrated HCl solution, exhibited higher thermal stability in comparison to pristine MWCNTs. The presence of magnetite, minor phase of metallic iron and cementite phases in as-synthesized nanomaterial reduced at 500°C facilitated the MWCNT decomposition and decreased the initial temperature of decomposition rate (Fig.S2, ESI†). This experiment also showed that the unpurified material showed total loss of weight of 92 % which means that the MWCNTs contain about 8% wt. of iron compounds. It is worth nothing that in the case of MWCNTs systems purified in HCl and reduced at 500°C the total loss of weight during the decomposition process is nearly 100% which suggests that only small part of iron species could have remained in the MWCNTs.

The catalytic activity of pristine, reduced, purified and purified and reduced MWCNTs was evaluated in ASRM. In order to elucidate the influence of the catalyst on the course of the investigated process additional measurements without catalyst were performed at 350 and 400 °C. The reactivity results expressed as methanol conversion, yield of hydrogen and selectivity to carbon dioxide, carbon monoxide and dimethyl ether (DME) are given in Figure 2, 3 and 4, respectively. The catalytic results showed that the ASRM reaction performed without the catalyst at 350 °C proceeds with low yield as evidenced by the low degree of methanol conversion (10%). Increasing the process temperature to 400 °C significantly increases the degree of methanol conversion up to 42% (see Fig. 2). It is also worth noticing that in the case of the reaction carried out at 350 °C only hydrogen and carbon dioxide as a major product of the ASRM process were formed. While, at higher temperature of the reaction formation of carbon monoxide was also observed. Carbon monoxide formation proves, that the decomposition of methanol and RWGS reaction during the ASRM process took place simultaneously (see Fig. 4)[11, 15]. The lack of the CO in the product of the ASRM reaction performed at 350 °C confirms that the reaction proceeds slightly. In addition, the high yield of hydrogen formation in the case of reaction performed at 400 °C confirmed the WGS reaction which runs during the ASRM process (see Fig. 3).

When the process was conducted using a catalyst the highest conversion of methanol was derived from MWCNTs activated in a mixture of 5%H_2-95%Ar at 500°C and demonstrated that H_2 and CO_2 are the major products in ASRM reaction. Besides the main products, the formation of undesired by-products such as carbon monoxide and DME were also observed (see Fig. 4). This result indicates that oxy-steam reforming of methanol was the major reaction which take place during the process. In addition, the presence of carbon monoxide and DME in the product indicates that the RWGS reaction and methanol decomposition run simultaneously during the ASRM process.

The catalytic activity tests showed that the purification of MWCNTs significantly influenced their catalytic activity, yield of hydrogen and selectivity towards obtained products. The purification of MWCNTs leads to decrease in methanol conversion. The MWCNTs which were only reduced, exhibited the highest activity in comparison to pristine MWCNTs and for these that were purified or purified and reduced. Purified MWCNTs before and after reduction exhibited comparable value of methanol conversion and hydrogen yield. These results confirmed that iron species such as Fe_3O_4 and metallic iron play crucial role in catalysing the ASRM reaction. The highest activity of reduced MWCNTs is most likely due to their highest content of iron species such as metallic iron, cementite and magnetite phase (see Fig. 5A). The reduction process carried out for the pristine material caused the reduction of surface and encapsulated iron (III) oxide particles to metallic iron or/and magnetite Fe_3O_4 phase (see Fig. 5B).

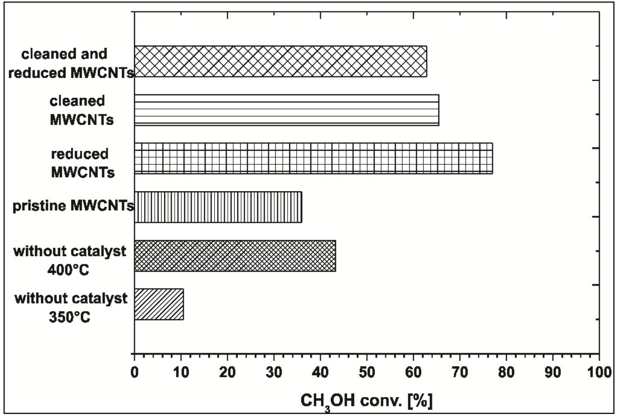

Fig.2 Methanol conversion for pristine MWCNTs, MWCNTs after reduction in 5%H_2-95%Ar mixture at 500 °C, after cleaning with HCl and after cleaning with HCl and reduction in 5%H_2-95%Ar mixture at 500 °C, respectively. ASRM reaction parameters: H_2O:O_2:CH_3OH = 1:0.4:1, weight of catalyst m = 0.1 g, p= 1bar, T = 350 °C and at 400°C for the process performed without catalyst.

View Article Online
DOI: 10.1039/C6RA15618E

It should be mentioned that during the purification process, defects may have been introduced on the exterior and interior wall on the carbon nanotubes in locations from which the iron species have been removed.

The differences in methanol conversion can be attributed to the structure modifications inside of the CNTs or/and change in the phase composition within the nanomaterial. Encapsulated nanoparticles inside the carbon nanotubes modify their electronic and magnetic properties as well as the carbon nanotubes themselves.

The nature and strength of the interaction between metal particles and carbon nanotubes depends on the metal. Whereas, the strength of the interaction between metal and CNT increases with the number of unfilled d-orbitals of the metal particle[17]. It is known that metals with closed shell such as gold and palladium exhibit very low affinity for carbon bonding. Iron, which has a few vacant d-orbitals, exhibit high affinity and certain solubility in carbon[17]. The electron structure of iron suggests that it is possible that during the synthesis of MWCNTs iron particles may be built into the structure of the carbon nanotubes and may even create iron carbides (e.g. Fe_3C). We observed the formation of Fe_3C during CVD synthesis of MWCNTs as well as iron (III) oxide and cementite (see Figure 5A).

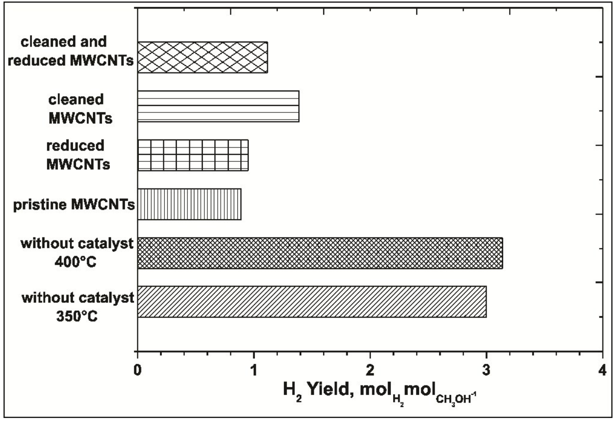

Fig.3 Yield of hydrogen production for pristine MWCNTs, MWCNTs after reduction in 5%H_2-95%Ar mixture at 500 °C, after cleaning with HCl and after cleaning with HCl and reduction in 5%H_2-95%Ar mixture at 500 °C, respectively. ASRM reaction parameters: H_2O:O_2:CH_3OH = 1:0.4:1, weight of catalyst m = 0.1 g, p= 1bar, T = 350 °C and at 400°C for the process performed without catalyst.

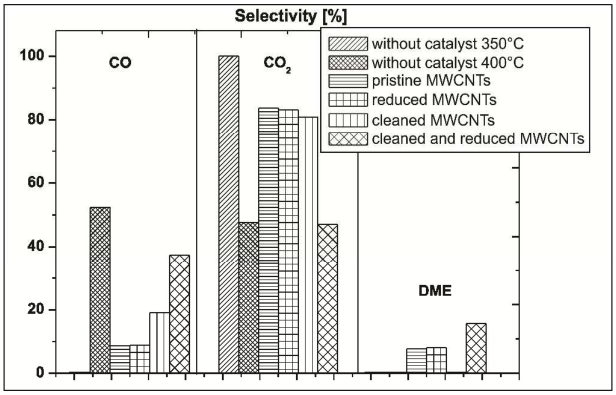

Fig.4 Selectivity towards CO, CO_2 and DME formation in ASRM reaction for pristine MWCNTs, MWCNTs after reduction in 5%H_2-95%Ar mixture at 500 °C, after cleaning with HCl and after cleaning with HCl and reduction in 5%H_2-95%Ar mixture at 500 °C, respectively. ASRM reaction parameters: H_2O:O_2:CH_3OH = 1:0.4:1, weight of catalyst m = 0.1 g, p= 1bar, T = 350 °C and at 400°C for the process performed without catalyst.

A covalent bond between metal particles and carbon nanotubes is formed by overlapping of p_z orbitals of carbon belonging to the graphene sheets and the unfilled d orbitals of the metal. These interactions may be further enhanced by the presence of defects such as carbon vacancies originating from extra curvature of the introduced in the nanotubes wall pentagon and heptagon rings.

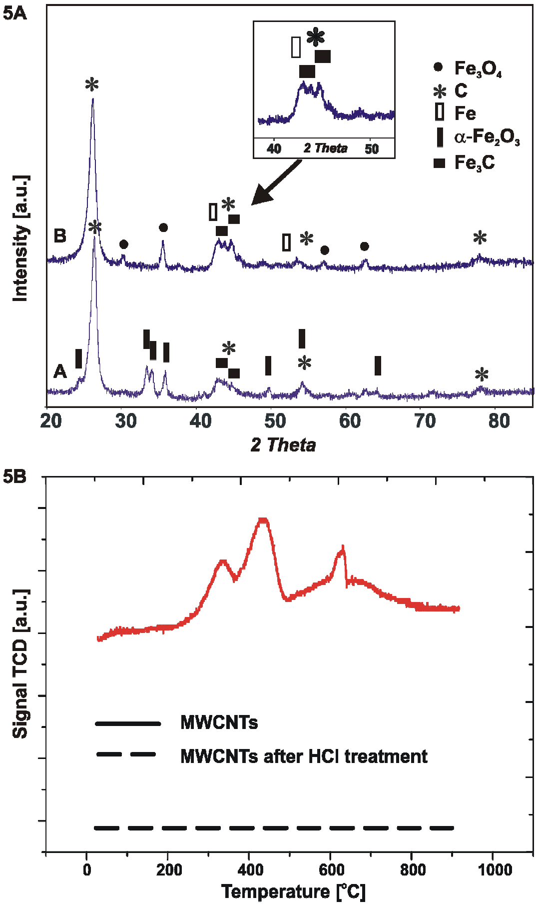

Fig.5. 5A) XRD measurements for A) pristine MWCNTs and B) pristine MWCNTs after reduction at 500 °C in 5%H_2-95 %Ar mixture and reaction, 5B) TPR profiles of pristine MWCNT and MWCNT cleaned with HCl solution.

The presence of metal particles inside of the CNT close to such defects can generate stronger interactions compared metal particle on the outer surface of the CNT. Metal particles inside the carbon nanotubes are decorated with layers of graphene sheets at the CNT side growth, the result of strong interactions between the metal particles and the first graphene sheet[17]. The geometrical structure of CNTs can be also affected by the interaction with another CNT or a metal surface. Additionally, the surface van der Waals forces could influence on MWCNTs structure[18] and can induce a decrease of MWCNTs diameter up to 30%. This is supported by a study of Muthaswami et al.[19] reporting that some chemical and physical properties of carbon nanotubes are induced by the defects created as a result of encapsulated of metal particles or by defects located at the tip or inside of the CNT.

View Article Online
DOI: 10.1039/C6RA15618E

The catalytic tests performed for all catalysts at 350 °C showed that the highest hydrogen yield in ASRM had catalytic materials which were cleaned or cleaned and reduced before activity test. Those systems also showed the lowest selectivity to CO_2 and the highest selectivity to CO formation. The selectivity to DME was also measured (see Fig. 4). The selectivity results showed that the lowest selectivity to DME close to zero per cent exhibited catalyst which undergone cleaning processes. This suggests that iron species may have significant influence on DME formation during the reaction.

The activity results confirmed that ASRM proceeds easier on reduced MWCNT containing metallic iron and magnetite. Carbon nanotubes could promote electron transfer in the reduction process and destabilize the α-Fe_2O_3 bonds and facilitate the reduction process of hematite to metallic iron and magnetite which enhances the catalytic activity. Cleaning of the nanotubes with HCl may introduce structural defects inside of the tube, which had significant influence on the catalytic activity of MWCNT in ASRM[20]. Gayathri et al.[21] studied hydrogen adsorption in carbon nanotubes defects and reported that defects in different types and sizes carbon nanotubes have an important contribution to the adsorption mechanism. These defects affect on hydrogen storage capacity by CNTs. These reports support the hypothesis that CNTs purified in HCl, can adsorb hydrogen which facilitate the ASRM.

In order to further clarify the catalytic activity of MWCNT, the surface adsorbed species formed during methanol decomposition over differently treated MWCNT (reduced only, purified and purified and reduced) were investigated by FTIR spectroscopy. IR spectra of adsorbed species taken after exposure of MWCNT only after reduction and after cleaning and reduction process collected at 350 and 400 °C are shown in Figure S3 (Fig.S3, ESI†). The IR spectra recorded for nano-system reduced at 500 °C showed several characteristic bands. The visible bands located at 830, 930, 1020, 1060, 1080, 1370, 1390, 1450, 1500, 1590, 1640, 1740, 2000, 2040, 2180, 2320, 2360, 3580, 3615, 3640–3670, 3700 cm^{-1} were observed both for the cleaned and none cleaned samples. The visible bands located at 1370 cm^{-1}, 1390 cm^{-1} and 1590 cm^{-1} were attributed to symmetric O-C-O stretching, CH deformation mode and asymmetric stretching of the O-C-O band intensity of formates species [22, 23]. In addition to the foregoing formate surface species, the bands assigned to the metoxy species can be found on the IR spectrum at a following positioned: 1060 cm^{-1} and 1450 cm^{-1}. Carbonate species were also detected visible at the following wavelengths: 830 cm^{-1}, 1020-1090 cm^{-1} (1020 cm^{-1}, 1080 cm^{-1}), 1570–1440 cm^{-1} (1500 cm^{-1}). In addition the band situated at 1636 cm^{-1} is attributed to C=C stretching, while the IR band situated at 1740 cm^{-1} is attributed to C=O stretching. Whereas, the bands situated at 2000 and 2040 cm^{-1} were assigned to carbonyl species due to CO adsorption[24]. Moreover, on the IR spectrum the appropriate bands seen at 2180 cm-1 attributed to gaseous CO and gaseous CO_2 assigned to the bands positioned at 2360 and 2320 cm-1 were also detected during the exposure of the investigated systems to a 1 vol.% methanol in an argon mixture[25]. The IR spectra collected during decomposition of methanol carried out at 350 and 400 °C showed also several bands located in the wavenumber range 3700 - 3580 cm^{-1} (3580 cm^{-1}, 3615 cm^{-1}, 3640 cm^{-1}, 3670 cm^{-1}, 3700 cm^{-1}) which were attributed to the free, non-associated -OH stretching frequencies present in the molecule of alcohol [26].

In order to better visualize the differences in the absorption species taken after reduction at 500°C in a 5%H_2-95%Ar mixture and exposure of the pristine MWCNT and MWCNT cleaned with HCl to a 1 vol.% methanol-argon mixture at 350 °C the IR spectra of the adsorbed species for both systems and difference spectrum of these spectra were presented in Figure 6. The system, which was purified in concentrated HCl solution, exhibited lower intensity bands assigned to surface species observed during the decomposition of methanol what can be easily seen on the difference spectrum.

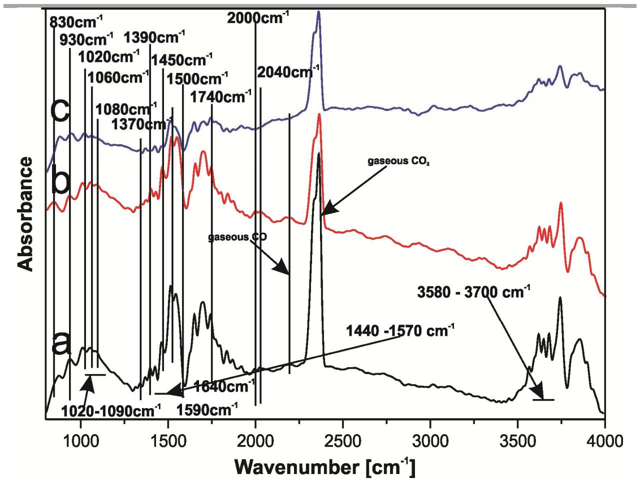

Fig.6 FTIR spectra of adsorbed species taken after reduction at 500 °C and exposure to a 1 vol.% methanol-argon mixture at 350 and 400 °C of the following catalytic systems a) pristine MWCNT b) MWCNT cleaned with HCl c) the difference spectrum a-c.

This result provides an explanation of the differences in reactivity of purified and pristine CNTs in oxy-steam reforming of methanol. The lower intensity of surface species in the case of MWCNTs after purification and reduction attributed to gaseous CO_2, formate, methoxy and carbonate species explain the lower methanol conversion and CO_2 selectivity in ASRM process.

In summary, this report demonstrates the potential of CNTs to serve as a potent catalyst in hydrogen generation. We have confirmed that the Fe_3O_4, metallic iron and defects formed by encapsulated or removal of metal particles play significant role in the oxy-steam reforming of methanol. TG results indicated that the presence of iron nanoparticles inside the carbon nanotubes facilitates their decomposition. The reduced MWCNTs exhibited excellent performance in ASRM and showed the highest methanol conversion efficiency at 350 °C and the highest selectivity to CO_2. In parallel reduced MWCNTs also showed the lowest selectivity towards the formation of CO. This phenomenon is explained by the presence of metallic iron and magnetite phases, which have significant influence on the catalytic activity of MWCNTs in ASRM. This report points out to novel unexplored opportunities in designing simple but effective catalytic systems for hydrogen generation.

Experimental: Multi-walled carbon nanotubes were synthesized by catalytic decomposition of hydrocarbon gas using chemical vapor deposition (CVD) method as described previously[27, 28]. Briefly, the MWNTs were home-made by pyrolyzing 5 wt.% of ferrocene in toluene mixture at 850°C in an Ar atmosphere. As-produced material consists of carpet-like structures containing highly oriented nanotubes of uniform diameter. The MWCNTs were cleaned twice using concentrated HCl solution for 12 h. Through this process most of the iron containing particles was removed from the MWCNTs. In the next step the MWCNTs were washed with deionized water until the pH was around 7, filtered and dried at 120 °C for 6 h. The TPR-H_2 measurements were carried out in an automatic TPR system

View Article Online
DOI: 10.1039/C6RA15618E

(Altamira AMI-1) in the temperature range 25-900 °C with linear heating rate 10 °C min^{-1} (weight about 0.1 g, reductiong mixture 5% H_2-95% Ar). Thermo-gravimetric TG method, equipped with differential thermal analysis DTA device MOM Budapest derivatograph (type 34-27T 1000 °C) was used for temperature programmed decomposition of carbon nanotubes in air atmosphere. Room temperature powder X-ray diffraction patterns were collected using a PANalytical X'Pert Pro MPD diffractometer in Bragg-Brentano reflecting geometry. Copper CuK_α radiation from a sealed tube was utilized. Data were collected in the range of 5-90° 2θ with step 0.0167° and exposure time per step of 27 s. Due to the fact that raw diffraction data contain some noise, the background during the analysis was subtracted using a Sonneveld, E.J. and Visser algorithm. The data was then smoothed using a cubic polynomial. All calculations were performed with X'Pert HighScore Plus computer program. Infrared spectra were recorded with a IRTracer-100 FTIR (Shimadzu) spectrometer equipped with a liquid nitrogen cooled MCT detector. Before analysis the sample was reduced at 500 °C in a 5%H_2-95%Ar stream (50 cm^3 min^{-1}). A resolution of 4.0 cm^{-1} was used throughout the investigation. 128 scans were taken to achieve a satisfactory signal to noise ratio. The background spectrum was collected at 100 °C after the reduction process. Then the reducing mixture was shifted to a mixture of approximately 1 vol.% CH_3OH in argon stream and spectra were collected at 350 and 400 °C. The decomposition process involved exposure of the reduced catalysts to 1 vol. % CH_3OH in argon stream flowing at 50 cm^3 min^{-1} for 30 min at 350 and 400 °C under atmospheric pressure. The catalytic activity in the oxy-steam reforming of methanol reaction was measured in a quartz flow microreactor. About 0.1 g of catalyst was loaded into a microreactor for the catalytic measurements. The reaction conditions were as follows: reaction temperature 350 °C, ratio of $CH_3OH:H_2O:O_2$ = 1:1:0.4, flow rate 31.5 cm^3 min^{-1}, atmospheric pressure. Methanol vapour or water vapour were introduced by bubbling argon buffer gas through two saturators filled with methanol or water, respectively. Whereas, oxygen was added using a mixture of 5%O_2-95%Ar to the stream directly before the reaction to avoid undesirable interaction of the reactants in the saturator. The catalytic activities are averages of three measurements and were determined after 2 h of time on-stream. The product stream was analyzed online using three gas chromatographs. Material balances on carbon were calculated to verify the obtained results. CH_3OH conversion and H_2 yield was calculated by the following equations:

$$CH_3OH \text{ conv.} = [(FCH_3OH \text{ in} - FCH_3OH \text{ out}) / (FCH_3OH \text{ in})] \times 100\ \%;$$

$$\text{yield of } H_2\text{: } YH_2 = (FH_2 / (FCH_3OH \text{ in} - FCH_3OH \text{ out}));$$

$$SCO_2 = (FCO_2/(\textstyle\sum F \text{ carbon containing product})) \times 100\ \%;$$

$$SCO = (FCO/(\textstyle\sum F \text{ carbon containing product})) \times 100\ \%;$$

$$S_{DME} = (F_{DME}/(\textstyle\sum F \text{ carbon containing product})) \times 100\ \%;$$

where: FH_2 = the molar flow rate of H_2 (mol min^{-1}), FCO = the molar flow rate of CO (mol min^{-1}), FCO_2 = the molar flow rate of CO_2 (mol min^{-1}), F_{DME} = the molar flow rate of dimethyl ether (mol min^{-1}), FCH_3OH out = the molar effluent rate of the CH_3OH feed out (mol min^{-1}) and FCH_3OH in = the molar flow rate of the CH_3OH feed in (mol min^{-1}).

Acknowledgments

The project was funded by the National Science Center (Grant no. DEC-2012/05/D/ST8/02856).

Notes and references

1. P. Mierczynski, K. Vasilev, A. Mierczynska, W. Maniukiewicz and T. Maniecki, *Topics in Catalysis*, 2013, **56**, 1015-1025.
2. P. Mierczynski, K. A. Chalupka, W. Maniukiewicz, J. Kubicki, M. I. Szynkowska and T. P. Maniecki, *Applied Catalysis B: Environmental*, 2015, **164**, 176-183.
3. P. Mierczynski, K. Vasilev, A. Mierczynska, W. Maniukiewicz and T. P. Maniecki, *Applied Catalysis A: General*, 2014, **479**, 26-34.
4. P. Mierczynski, K. Vasilev, A. Mierczynska, W. Maniukiewicz, M. I. Szynkowska and T. P. Maniecki, *Applied Catalysis B: Environmental*, 2016, **185**, 281-294.
5. R. S. Cherry, *International Journal of Hydrogen Energy*, 2004, **29**, 125-129.
6. M. A. Ebiad, D. R. Abd El-Hafiz, R. A. Elsalamony and L. S. Mohamed, *RSC Advances*, 2012, **2**, 8145-8156.
7. R. Chakrabarti, J. S. Kruger, R. J. Hermann and L. D. Schmidt, *RSC Advances*, 2012, **2**, 2527-2533.
8. X. Zhang, S. H. Chan, H. K. Ho, S.-C. Tan, M. Li, G. Li, J. Li and Z. Feng, *International Journal of Hydrogen Energy*, 2015, **40**, 6866-6919.
9. K. Geissler, E. Newson, F. Vogel, T.-B. Truong, P. Hottinger and A. Wokaun, *Physical Chemistry Chemical Physics*, 2001, **3**, 289-293.
10. R. Perez-Hernandez, G. Mondragon-Galicia, A. Allende Maravilla and J. Palacios, *Physical Chemistry Chemical Physics*, 2013, **15**, 12702-12708.
11. P. Mierczynski, R. Ciesielski, A. Kedziora, M. Nowosielska, J. Kubicki, W. Maniukiewicz, A. Czylkowska and T. Maniecki, *Reaction Kinetics, Mechanisms and Catalysis*, 2015, 1-17.
12. R. Barthos and F. Solymosi, *Journal of Catalysis*, 2007, **249**, 289-299.
13. H.-M. Yang and P.-H. Liao, *Applied Catalysis A: General*, 2007, **317**, 226-233.
14. P. K. Seelam, M. Huuhtanen, A. Sápi, M. Szabó, K. Kordás, E. Turpeinen, G. Tóth and R. L. Keiski, *International Journal of Hydrogen Energy*, 2010, **35**, 12588-12595.
15. P. Mierczynski, K. Vasilev, A. Mierczynska, W. Maniukiewicz, R. Ciesielski, J. Rogowski, I. M. Szynkowska, A. Y. Trifonov, S. V. Dubkov, D. G. Gromov and T. P. Maniecki, *Catalysis Science & Technology*, 2016, **6**, 4168-4183.
16. E. R. Edwards, E. F. Antunes, E. C. Botelho, M. R. Baldan and E. J. Corat, *Applied Surface Science*, 2011, **258**, 641-648.
17. J. Gallego, J. Barrault, C. Batiot-Dupeyrat and F. Mondragon, *Micron*, 2013, **44**, 463-467.
18. T. Hertel, R. E. Walkup and P. Avouris, *Physical Review B*, 1998, **58**, 13870-13873.
19. L. Muthaswami, Y. Zheng, R. Vajtai, G. Shehkawat, P. Ajayan and R. E. Geer, *Nano Letters*, 2007, **7**, 3891-3894.
20. S. Song, H. Yang, R. Rao, H. Liu and A. Zhang, *Catalysis Communications*, 2010, **11**, 783-787.
21. V. Gayathri and R. Geetha, *Adsorption*, 2007, **13**, 53-59.
22. G. Jacobs and B. H. Davis, *Applied Catalysis A: General*, 2005, **285**, 43-49.
23. M. A. Larrubia Vargas, G. Busca, U. Costantino, F. Marmottini, T. Montanari, P. Patrono, F. Pinzari and G.

View Article Online
DOI: 10.1039/C6RA15618E

Ramis, *Journal of Molecular Catalysis A: Chemical*, 2007, **266**, 188-197.
24. S. A. Mirji, S. D. Adyanthaya, V. Ravi, N. E. Jacob, R. K. Jha, K. R. Patil, R. S. Gholap and A. B. Gaikwad, *Colloids and Surfaces A: Physicochemical and Engineering Aspects*, 2007, **302**, 337-341.
25. P. Mierczynski, T. P. Maniecki, K. Chalupka, W. Maniukiewicz and W. K. Jozwiak, *Catalysis Today*, 2011, **176**, 21-27.
26. M. D. Ellison, S. T. Morris, M. R. Sender, J. Brigham and N. E. Padgett, *The Journal of Physical Chemistry C*, 2007, **111**, 18127-18134.
27. M. Pinault, V. Pichot, H. Khodja, P. Launois, C. Reynaud and M. Mayne-L'Hermite, *Nano Letters*, 2005, **5**, 2394-2398.
28. M. Pinault, M. Mayne-L’Hermite, C. Reynaud, V. Pichot, P. Launois and D. Ballutaud, *Carbon*, 2005, **43**, 2968-2976.

View Article Online
DOI: 10.1039/C6RA15618E